Publications

1-22-2019

Latitude and Longitude Dependence of Ionospheric Tec and Magnetic Perturbations From Infrasonic-Acoustic Waves Generated by Strong Seismic Events

M. D. Zettergren
Embry-Riddle Aeronautical University, zettergm@erau.edu

J. B. Snively
Embry-Riddle Aeronautical University, snivelyj@erau.edu

Latitude and Longitude Dependence of Ionospheric TEC and Magnetic Perturbations From Infrasonic-Acoustic Waves Generated by Strong Seismic Events

M. D. Zettergren[1] [ID] **and J. B. Snively**[1] [ID]

[1]Department of Physical Sciences and Center for Space and Atmospheric Research, Embry-Riddle Aeronautical University, Daytona Beach, FL, USA

Abstract A numerical study of the effects of seismically generated acoustic waves in the ionosphere is conducted using a three-dimensional (3-D) ionospheric model driven by an axisymmetric neutral atmospheric model. A source consistent with the 2011 Tohoku earthquake initial ocean surface uplifting is applied to simulate the subsequent responses. Perturbations in electron density, ion drift, total electron content (TEC), and ground-level magnetic fields are examined. Results reveal strong latitude and longitude dependence of ionospheric TEC, and of ground-level magnetic field perturbations associated with acoustic wave-driven ionospheric dynamo currents. Results also demonstrate that prior two-dimensional models can capture dominant meridional responses of TEC over latitude, even though dynamics at other longitudes are not resolved. Conclusions support that TEC and magnetic signatures can arise from nonlinear acoustic waves generated by strong earthquakes; simulations elucidate the comprehensive physics of their 3-D ionospheric responses.

Plain Language Summary This paper reports new numerical model results on how the ionosphere—the ionized, conducting region of the upper-atmosphere—responds to strong acoustic waves launched by earthquakes. The effects of these waves in the ionosphere can be observed from ground: They are measured as variations in Global Positioning System satellite signals received at the ground, which translate to variations in integrated electron content of the ionosphere. They can be detected also via small fluctuations in magnetic field, which are driven by ionospheric currents. The model results suggest that both measurement techniques can provide insight into the waves and their sources; new guidance for interpreting these measurements is provided. Further, results demonstrate a new capability for simulating these processes in three dimensions, which can be applied to more-realistic case studies.

1. Introduction

Atmospheric acoustic and gravity waves (AGWs) are readily generated by disturbances at ground-level or in the troposphere and propagate to—and strongly impact—the ionosphere-thermosphere-mesosphere (ITM) (Fritts & Alexander, 2003; Fritts et al., 2006, and references therein). Conservation of energy requires that AGW velocity perturbations grow in amplitude with decreasing density, and thus increasing altitude, until the onset of dissipation. They produce significant, measurable, and sometimes nonlinear disturbances in the ITM. Gravity waves (GWs) are generated by processes that result in vertical displacements of the stably stratified atmosphere over sufficiently large spatial and temporal scales. Seismic events (e.g., Matsumura et al., 2011) and tsunamis (e.g., Peltier & Hines, 1976) generate GWs as well as acoustic waves (AWs), which arise from processes that occur over time scales short enough to compress the atmosphere. The AWs that reach and impact the ITM exhibit infrasonic periods of approximately tens of seconds to minutes (approaching the acoustic cutoff frequency of the lower atmosphere) and are often identified following earthquakes (EQs; e.g., Matsumura et al., 2011) and volcanic eruptions (Dautermann et al., 2009).

Transient AWs are generated by initial ocean disturbances from undersea EQs, which also lead to tsunamis that serve as an efficient generator of GWs (e.g., Galvan et al., 2012; Kakinami et al., 2012; Rolland et al., 2011, and references therein). EQ-generated AWs are readily identifiable in Global Navigation Satellite System receiver derived total electron content (TEC) measurements as ~0.1–2 TECU, 3–5 mHz, oscillations, which are delayed from the EQ occurrence by the acoustic travel time from the ground to the

thermosphere-ionosphere. In some recent cases of strong EQs, the onset of acoustic oscillations is concurrent with a persistent, sharp decrease in TEC (as large as ~4–8 TECU) above the epicenter (Astafyeva et al., 2013; Kakinami et al., 2012; Saito et al., 2011). This TEC depletion occurs following acoustic shock waves, or non-linear acoustic ("sawtooth") wave trains, which drive transport processes in the IT (Shinagawa et al., 2013; Zettergren et al., 2017). Sustained acoustic oscillations at ~3.7-min period, lasting 30 min to 1 hr after the EQ have also been detected in TEC perturbations (Matsumura et al., 2011; Saito et al., 2011; Zettergren et al., 2017) and result from vertical acoustic resonance between the ground (or tropopause) and thermosphere.

Observations of magnetic fluctuations following seismic sources have also been reported (e.g., Iyemori et al., 2005) but are less common and well-understood than signatures in TEC. Iyemori et al. (2005) reported magnetic fluctuations following the M 9.1 26 December 2004 Sumatran EQ, including apparent geomagnetically conjugate signatures indicating interhemispheric coupling of dynamo currents. Similar to TEC disturbances, these fluctuations began ~12 min after the EQ, consistent with the AW travel time from the EQ fault to the ionosphere. They had a dominant frequency of ~4.5 mHz and amplitude of ~1–2 nT, peak-to-peak (PTP). Qualitatively similar TEC and magnetic fluctuations were also observed following the M 8.6 28 March 2005 Sumatran EQ (Hasbi et al., 2009).

AGWs generate dynamo electrical currents and, hence, magnetic perturbations, as they propagate through conducting ionospheric plasma layers at ~100–300-km altitude (e.g., Hao et al., 2013; Zettergren & Snively, 2013, 2015). Simulations of magnetic fluctuations due to seismic sources predict detectable fluctuations at AGW frequencies at ground-level (Kherani et al., 2012) and in the ionosphere (Imtiaz & Marchand, 2012). Detailed simulations by Zettergren and Snively (2015) found ground-level signatures ~0.1–2 nT in amplitude and in situ signatures are ~1–10 nT, which match the approximate characteristics of observations; however, simplified sources and two-dimensional (2-D) models were used that do not fully capture the geometry of wave-driven currents. Ionospheric currents generated by AWs are likely to have complex shape and character due to the anisotropic conductances and geomagnetic field directions. By comparison, the 2-D simulations use a sheet current approximation that may accordingly overestimate the AW-generated currents and magnetic fields.

Multiple other processes may contribute to EQ-related magnetic fluctuations (cf. Johnston, 1997, and references therein). Recent interest has focused on piezomagnetic effects associated with stress buildup and release in a fault before and during large EQs (e.g., Utada et al., 2011, and references therein). Tsunamis following large undersea EQs may also create magnetic perturbations via induced electric fields from the motion of electrically conducting seawater through the geomagnetic field, leading to electrical currents and local magnetic fluctuations (Utada et al., 2011). Although the M 9.1 11 March 2011 Tohoku EQ (Hao et al., 2012, 2013; Utada et al., 2011) apparently generated magnetic field fluctuations, there was additional evidence for coseismic magnetic perturbations. These fluctuations were not time-shifted by the acoustic travel time between the ground and ionosphere and may be due to piezomagnetic effects or to the tsunami-driven motions of seawater (Utada et al., 2011); this event also occurred during a period of moderate geomagnetic activity, which may provide another source of fluctuations.

Zettergren et al. (2017) emphasized the importance of nonlinearity in determining TEC signatures near the epicenter, while also noting clear evidence for latitudinal anisotropies in the observed ionospheric responses in TEC data and two-dimensional (2-D) model simulations; longitudinal anisotropies, however, were also identified in data. Recent investigations by Meng et al. (2018) address primary three-dimensional (3-D) TEC observables but do not consider the nonlinear formation of depletions, coupling along the geomagnetic field into the conjugate hemisphere, or magnetic fluctuations. Here we report the *structures of ionospheric responses and observables in latitude, longitude, and time following strong AW forcing by seismic hazard events*, using a controlled source designed for the 2011 Tohoku-Oki EQ (Zettergren et al., 2017). We leverage a new 3-D ionospheric model to resolve full TEC spatial dependence and magnetic field perturbations—capturing both linear and nonlinear aspects—alongside the distributed ionospheric responses, namely, density, drift, and currents, spanning from source to conjugate hemispheres.

2. Numerical Modeling Basis

The modeling approach used in this study is an extension of 2-D models described in Zettergren and Snively (2015, Appendix A). Specifically, the 3-D ionospheric <u>G</u>eospace <u>E</u>nvironment <u>M</u>odel for <u>I</u>on-<u>N</u>eutral <u>I</u>nteractions (GEMINI) and 2-D axisymmetric (rotated about the epicenter) neutral atmospheric <u>M</u>odel for
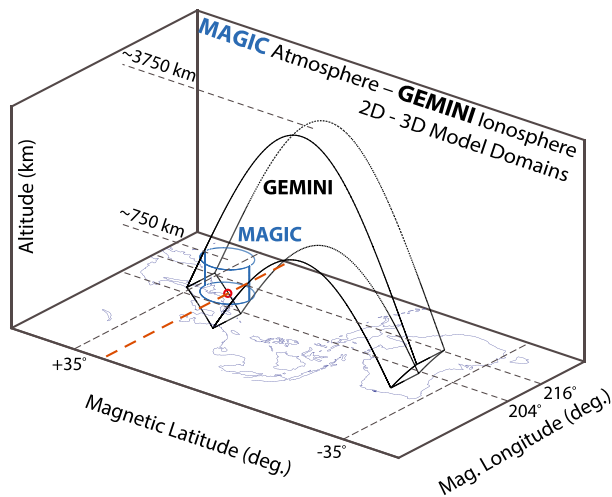
Figure 1. Neutral atmosphere (MAGIC) and ionosphere (GEMINI) grids used in this study. The epicenter for the 2011 Tohoku earthquake is marked by a red circle, the MAGIC grid extent is marked in blue lines, and the GEMINI grid extent is marked in black lines.

Acoustic and Gravity wave Interactions and Coupling (MAGIC) (Snively, 2013, and references therein) are applied. MAGIC solves the Euler equations via the *f* wave method of Bale et al. (2003) in a modified version of Clawpack 4.2 (Clawpack Development Team, 2002; LeVeque, 2002), with time-split solutions for Navier-Stokes viscosity and thermal conduction. *The symmetry of the 2-D axisymmetric wave field enables us to clearly isolate the 3-D features associated with the ionospheric response.* GEMINI uses the same mathematical formulation as Zettergren and Snively (2015, Appendix A) except for that the electrodynamic problem is changed slightly; the large number of grid points needed for this study makes both direct and iterative solutions inefficient, so we adopt an equipotential field line (EFL) approximation, which uses a field-integrated version of the current continuity equation (e.g., Huba et al., 2015). With the EFL setup, GEMINI computes field-aligned component of the current density from the divergence of the perpendicular components instead of directly from the potential. The EFL equation, similar to that presented in Zettergren et al. (2015), is solved using the MUMPS software (Amestoy et al., 2001, 2006).

Figure 1 illustrates the MAGIC and GEMINI domains for this investigation. Coupling of perturbations (neutral velocities, temperature, and species densities) from MAGIC to GEMINI is achieved by calculating modeled deviations from the empirical NRLMSISE00 atmospheres (Picone et al., 2002), used in both models, and time-dependently interpolating these into the ionospheric model.

GEMINI uses nonuniform grid spacing in the field-aligned direction to maintain high resolution in the source hemisphere, with decreasing resolution at very high altitudes and in the conjugate hemisphere. Resolution in the source ionospheric hemisphere is 1–3 km for GEMINI; the uniform MAGIC grid has 1-km resolution.

3. Results

Figure 2 shows plasma density and parallel drift velocity responses (at 6:03:53 UTC) following the 2011 Tohoku EQ (which occurred at 5:46:23 UTC). These plots show slices of plasma parameters in different planes cut through the 3-D model domain (see the caption for detailed explanation). Representative field lines in each plane are drawn in the ion velocity panels of Figures 2d–2f. Supplementary information for this article includes movies of both the plasma density (Movie S1) and drift responses (Movie S2) versus time based on results from this figure. Movie S3 shows the same ion drift results, but focused, for clarity, on the hemisphere of the EQ to elucidate details of the acoustic responses.

The AWs are nonlinear and arrive as a ~4-min oscillation (resonant at lower altitudes; e.g., Saito et al., 2011) exhibiting steepened phase fronts that may individually appear as shocks, which are then rapidly dissipated in the thermosphere (Zettergren et al., 2017). A strong second packet arrives shortly after, due to prior reflection. Similar waveforms were reported above the weaker 2016 Kaikoura EQ (Li et al., 2018), where leading nonlinear waves were observed before a weaker, trailing packet; the dominant features of these signatures may be explained simply by dispersion, steepening, and reflection (see Figures 7 and 9 of Zettergren et al., 2017).

The behavior of plasma density and velocity *in the meridian of the epicenter* (Figure 2a) is quantitatively similar to 2-D simulation results presented in Zettergren et al. (2017, Figure 3). Field-aligned plasma drifts exceed 300 m/s in the F region and exhibit clear nonlinear features (steepened phase fronts and background modifications) resulting in a strong downward field-aligned flow (positive in the plot) at this time. These drifts mirror the causative AW amplitudes and period up to ~450 km where ion-neutral collisions become less important, limiting coupling of the gases (see Zettergren & Snively, 2015). Density (Figures 2a and 2c) and drift (Figures 2d and 2f) responses are the strongest in the direction of the magnetic equator, and are symmetric in longitude (Figures 2b and 2e). This is due to favorable alignment of the AW velocities (mostly radial away from the epicenter) with the background geomagnetic field, which efficiently generates parallel ionospheric transport (due to large parallel ion mobility). Thus, the drift response is asymmetric in lati-
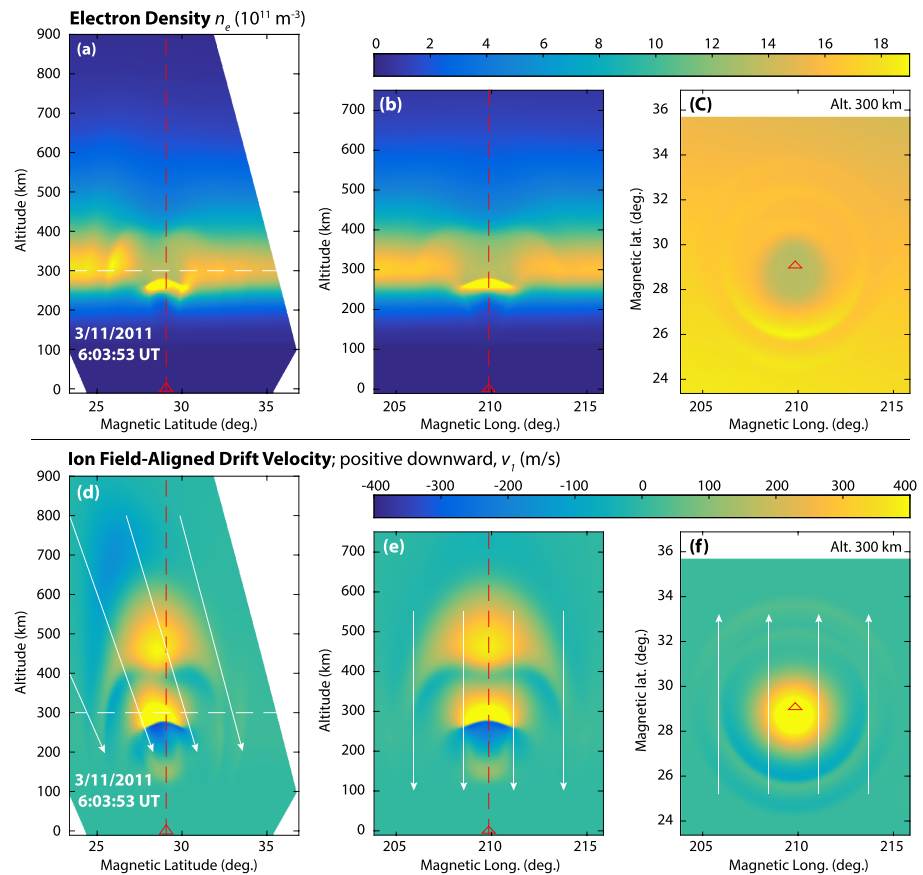
Figure 2. Simulated 3-D ionospheric density and field-aligned drift response for the 2011 Tohoku earthquake illustrating passage of the nonlinear acoustic wave through the F region ionosphere. (a) Plasma density in the source hemisphere in the magnetic meridian of the epicenter; (b) plasma density in the source hemisphere at the latitude of the epicenter; (c) plasma density in the source hemisphere as a function of latitude and longitude at an altitude of 300 km; (d) plasma field-aligned drift (positive in the direction of the geomagnetic field, "down-parallel" for the northern hemisphere) in the magnetic meridian of the epicenter; (e) plasma field-aligned drift at the magnetic latitude of the epicenter; and (f) plasma field-aligned drift versus latitude and longitude in the source hemisphere at an altitude of 300 km.

tude about the epicenter, and plasma density responses are stronger in the *equatorward* direction. Plasma drift and density responses are symmetric, in longitude, about the epicenter due to the fact that MAGIC was run in an axisymmetric configuration for this study (i.e., all asymmetries revealed are due to the *iono-spheric* dynamics). Thus, one can reasonably interpret *longitudinal* asymmetries in TEC perturbations as indicating asymmetry in either the seismic source or the background atmospheric conditions (affecting wave propagation).

Modeled current densities are modest in amplitude, ranging from ~0.2 μA/m^2 for the field-aligned current shown in Figures 3a and 3b to ~0.4 for the zonal currents shown in Figures 3f–3h, which tend to be the largest in the simulation. Supplementary movies related to this plot are included with this article as Movie S4–S6 and show the parallel current (J_1), the current along direction of increasing L-shell (J_2), and the zonal currents (J_3), respectively.

Relatively strong zonal currents (J_3) above the epicenter are produced by the lower F region dynamo (from the Pedersen conductance) which generates a current in the $\mathbf{v}_n \times \mathbf{B}$ direction (here zonal due to the pre-dominantly vertical wind forcing combined with strong horizontal geomagnetic field). Similarly, currents in the x_2 direction (in the direction of increasing L-shell) away from the epicentral longitude (Figures 3d and 3e) are also Pedersen in nature (at these locations, the $\mathbf{v}_n \times \mathbf{B}$ direction has a more meridional char-acter). Field-aligned currents close the perpendicular dynamo currents, insuring a divergence-free current system spanning both hemispheres (>50° of magnetic latitude). Conjugate (southern) hemisphere perpen-
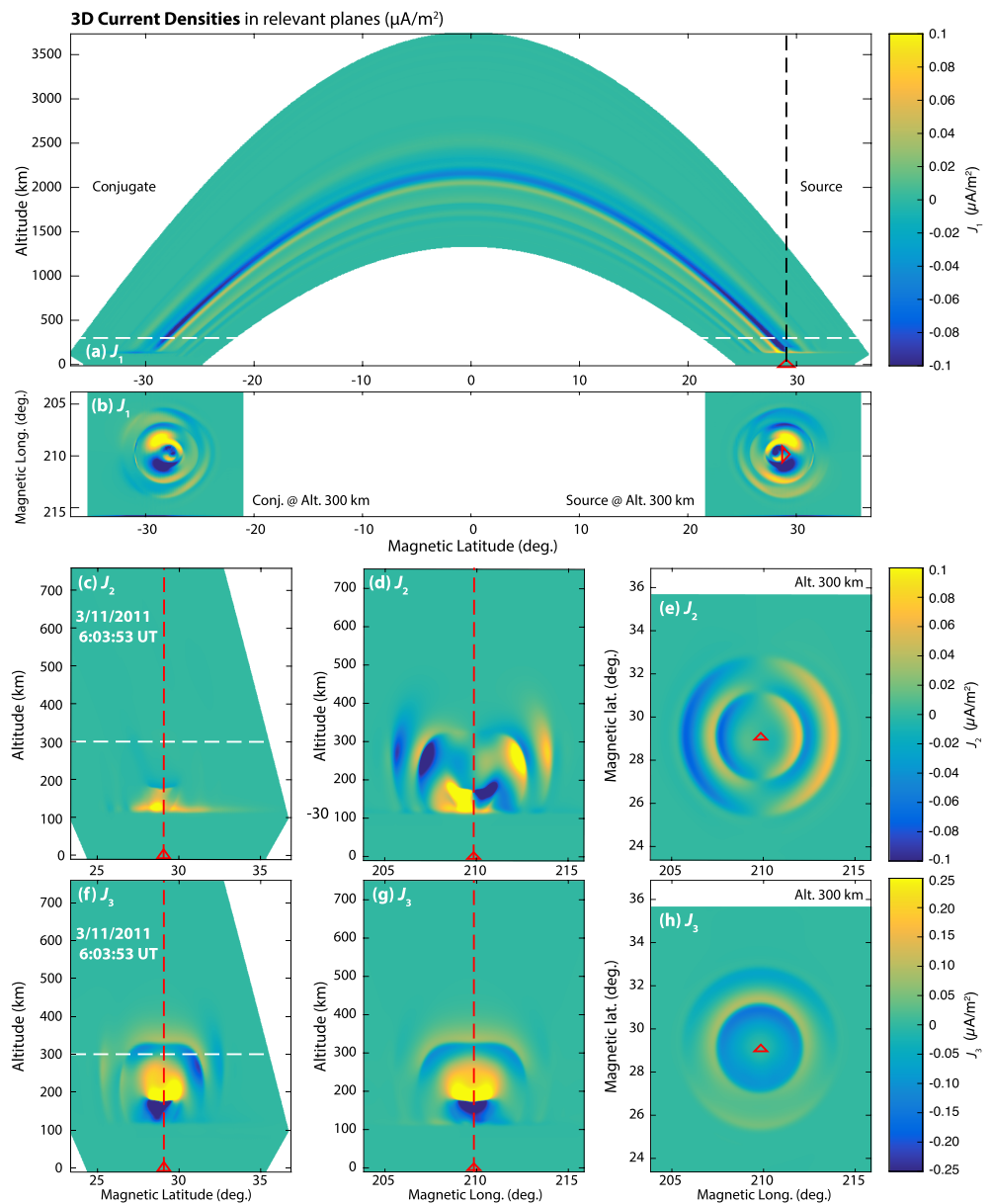
Figure 3. Simulated 3-D ionospheric current density response for the 2011 Tohoku earthquake illustrating passage of the nonlinear acoustic wave through the F region ionosphere. J_1 is the field-aligned (positive along the field direction) component of the current, J_2 is the component along the direction of increasing L-shell, and J_3 is the zonal current density. (a) Field-aligned current in the magnetic meridian of the epicenter; (b) field-aligned current at 300 km altitude; (c) J_2 in the meridian of the epicenter; (d) J_2 at the latitude of the epicenter; (e) J_2 at 300 km altitude; (f) J_3 in the meridian of the epicenter; (g) J_3 at the latitude of the epicenter; and (h) J_3 at 300 km altitude.

dicular currents (seen in Movies S5 and S6) complete the system and indicate the existence of an electric field spanning both hemispheres. In addition to driving the conjugate perpendicular currents, these fields cause significant (order m/s) $\mathbf{E} \times \mathbf{B}$ drifts and plasma redistribution which, as shown later in Figure 4, induce conjugate TEC perturbations. It is worth noting that the electric field generated by the AW will depend on both source and conjugate hemisphere conductances, hence, background ionospheric state, as determined by location, geomagnetic activity, and time of day. In contrast to density and velocity perturbations (Figure 2), the field-aligned currents (Figures 3a and 3b) tend to be the largest in the poleward and in the magnetic east-west directions away from the (ionospheric) epicenter. The current in the x_2 direction is the largest east and west of the epicenter (Figures 3d and 3e), while the zonal current perturbations seem to be more circularly symmetric (e.g., Figure 3h).
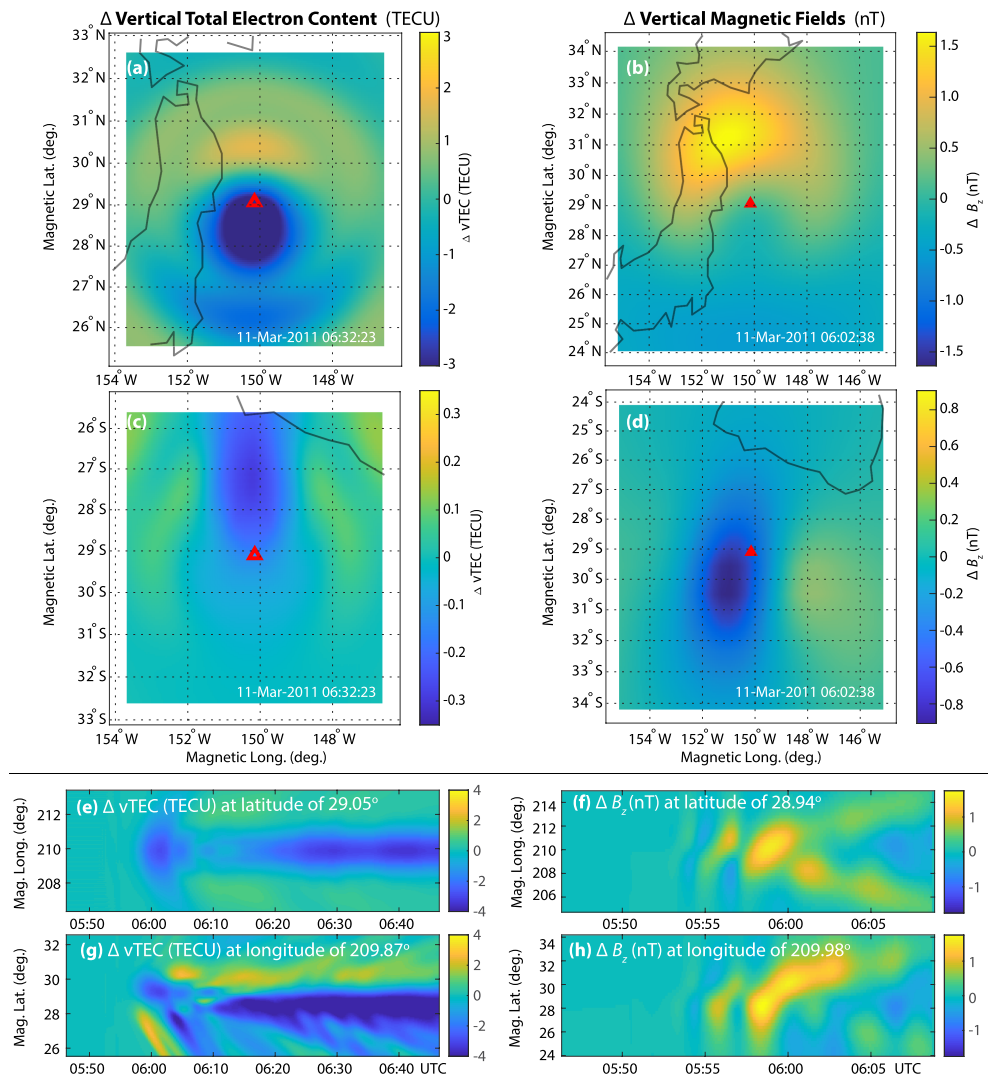
Figure 4. Simulated observable responses to the 2011 Tohoku earthquake. (a) A snapshot in time of TEC in the hemisphere of the earthquake (epicenter marked by a red triangle); (b) a snapshot of vertical magnetic fluctuations in the source hemisphere; (c) a snapshot of conjugate TEC fluctuations (the epicenter conjugate point is marked by a red triangle); (d) a snapshot of conjugate vertical magnetic field; (e) TEC versus longitude and time; (f) vertical magnetic field versus longitude and time; (g) TEC versus latitude and time; and (h) vertical magnetic field versus latitude and time.

Directionality of the current and perpendicular dynamo field responses can also be explained as an effect of background geomagnetic field on ion mobilities. Referencing the field line diagrams shown in Figure 2, it can be seen that, away from the epicentral longitude, radially directed AW velocity perturbations (not shown) are mostly perpendicular to the geomagnetic field illustrated in the plot. This is a favorable alignment for generating dynamo currents that depend on *perpendicular* neutral forcing (Zettergren & Snively, 2015, equation A14). Additionally, poleward of the epicenter, the field lines are mostly perpendicular to the AW velocities again favoring dynamo current generation. Conversely, the plasma *parallel* drift responses tend to be the largest where AW forcing aligns with the geomagnetic field (equatorward; Zettergren & Snively, 2013, 2015, and along the meridian of the source). Overall, *plasma drifts are mostly parallel/antiparallel to geomagnetic field lines*; perpendicular forcing is comparatively weak yet still notable as generates electrical responses in the ionosphere. Quantitative descriptions of spatial structure are more difficult to make than for the plasma density and drift since there are currents both from direct neutral forcing and from the dynamo fields that result. This interplay likely has some effect on the complicated spatial dependence of the current structures shown in Figure 3.

Figure 4 shows the observable ionospheric responses of ground-level magnetic field and TEC perturbations. Perturbations are computed from GEMINI by subtracting results from simulations conducted without EQ forcing. Snapshots of source hemisphere and conjugate hemisphere (vertical) magnetic field and TEC are shown in Figures 4a and 4c, and 4b and 4d, respectively. The time-dependent character of these oscillations is shown in Figures 4e and 4g for the magnetic field and 4f and 4h for the TEC. Movies S7–S14 are related to results shown in this diagram and include source hemisphere TEC, conjugate TEC, source hemisphere vertical magnetic field, source hemisphere southward magnetic field, source hemisphere zonal magnetic field, conjugate vertical magnetic field, conjugate southward magnetic field, and conjugate zonal magnetic field, respectively.

A pronounced TEC depletion (about −4.5 TECU) with accompanying fluctuations at AW periods can be seen near the epicenter in Figures 4a, 4c, 4e, and 4g. In Figures 4a and 4g, a preference for strong equatorward perturbations reflects the efficient ion-neutral coupling in this direction. Features of the meridional TEC responses evident in Figure 4h have been noted in 2-D simulations (Zettergren et al., 2017); it appears that a 2-D, meriodional slice approach for ionospheric modeling is reasonable for studying some of the latitudinal structures of TEC fluctuations.

The TEC fluctuations versus longitude near the source latitude—see Figure 4a—are generally smaller, particularly away from the epicenter, than the fluctuations shown in the latitude-time plot in Figure 4b, ostensibly due to the relatively perpendicular alignment of the AW velocities and geomagnetic field as one moves away from the longitude of the EQ. The TEC responses versus longitude are symmetric about the epicenter and appear localized within a few degrees longitude of the epicenter. TEC perturbation frequencies and wavelengths approximately correspond to those of the causative AWs, although there is some masking of the spatial structure of the waves due to nonlinear distortion in the wave fronts. The directivity of the waves also leads to more planar phase fronts that reach the ionosphere at similar times in locations spread across a range of latitudes and longitudes. This can result in slightly faster apparent phase speeds in the TEC perturbations versus the actual AWs (Zettergren & Snively, 2015).

Figures 4b, 4d, 4f, and 4h show the geomagnetic field perturbations at ground level due to the AW-generated dynamo currents (e.g., Figure 3). Geomagnetic field perturbations are computed from ionospheric currents in GEMINI; thus, they isolate magnetic effects of AWs and do not include effects of the tsunami or piezomagnetic effects (Johnston, 1997). Fields produced by ionospheric dynamo effects initially have very complicated nondipolar structure (see also rotation of features in the field components in Movies S9–S11)—consistent with the complicated field-aligned current structures shown in Figure 3. Vertical and meridional fields have somewhat larger perturbations, suggesting that the strongest currents affecting ground-level field are the zonal ionospheric currents, as expected from Figure 3. The magnetic field perturbations maximize at ∼1.5–2 nT PTP which is roughly consistent with reported observations of magnetic fluctuations following the 2011 Tohoku EQ (Hao et al., 2013; Utada et al., 2011). Generally, observations seem to indicate the presence of ∼1 nT amplitude perturbations following very large EQs like recent Sumatran EQs (Hasbi et al., 2009; Iyemori et al., 2005) and Tohoku (Hao et al., 2013; Utada et al., 2011); however, the observed timing and frequency content of the magnetic perturbations is complicated by the potential presence of sources other than the AWs that we simulate here.

Interhemispheric effects of AGWs excited by natural hazard events have been suggested in prior studies (e.g., Huba et al., 2015; Iyemori et al., 2005; Zettergren & Snively, 2013, 2015). Ion sound waves (Huba et al., 2000) in the F region and topside ionosphere travel along the geomagnetic field line toward the opposite hemisphere (particularly visible in the later frames of Movie S2). These are excited by neutral perturbations near the F region peak which drive ion motions at higher altitude where the gases decouple, thus forming compressional plasma waves of similar frequency (cf. also Zettergren & Snively, 2015). Electric fields are generated by the strong AW forcing and map between hemispheres in the simulation. Due to the quasi-electrostatic nature of our simulation, this mapping occurs instantly in the model, whereas, in nature, it would occur at the Alfvén speed. These fields create TEC variations in the conjugate ionosphere via $\mathbf{E} \times \mathbf{B}$ drifts (Figure 4d) which move plasma into regions where chemical balance is altered, thus changing plasma density. Conjugate TEC variations are about 0.35 TECU PTP, smaller than those in the source hemisphere by a factor of ∼10; however, these may be detectable given suitably quiet background wave activity. Spatial structure in the conjugate fluctuations is very different from the source hemisphere, since only the electric field contributes to transport and TEC variations; in contrast, direct neutral-ion momentum transfer largely

controls the source hemisphere responses. Conjugate TEC perturbations retain very little of the wave structure apparent in the source (northern) hemisphere but do form a mild TEC depletion near the end of the simulation (about an hour after the EQ). Finally, it is noted that weak conjugate magnetic field fluctuations (0.5–1 nT PTP) also exist in the simulations; these are only ∼3–5 times weaker than those in the source hemisphere, indicating somewhat efficient long-range conveyance of the electrical perturbations by AWs, as compared to TEC variations.

4. Discussion and Concluding Remarks

Detailed simulations of ionospheric plasma density, drift, and electrodynamic responses to the 2011 Tohoku EQ-generated nonlinear AWs were conducted using a new 3-D ionospheric model (GEMINI) coupled to an axisymmetric neutral dynamics model (MAGIC). Plasma density and drift exhibit similar asymmetric features, in the meridional plane, to 2-D simulations of Zettergren et al. (2017); however, they exhibit zonally symmetric responses (for a symmetric wave source in a windless atmosphere). The TEC variations in our 3-D model also mirror, in the meridional plane, those of Zettergren et al. (2017) and thus indicate that 2-D simulations in the meridional plane may be adequate for studying TEC fluctuations in their source hemisphere. In present and prior studies of the Tohoku EQ, both linear and nonlinear atmospheric and ionospheric responses have been found necessary to describe basic features of the observed TEC fluctuation signatures.

Perturbations in magnetic field on the ground due to the AW-dynamo currents are found to be ∼ 0.5–2 nT PTP and would be detectable with some types of sensitive magnetometers and suitably quiet background conditions. This supports a role for *ionospheric currents* in producing geomagnetic perturbations observed following strong EQs (Hao et al., 2013), which may be coincident with other sources of field fluctuations (e.g., piezomagnetic effects and tsunami-generated electrical currents in the ocean; Johnston, 1997). Interhemispheric coupling via electric fields occurs in our 3-D simulations and generates small but potentially detectable conjugate perturbations in TEC. Conjugate geomagnetic perturbations exist, are smaller than those in the source hemisphere, and are potentially detectable under favorable conditions. The conjugacy of magnetic field and TEC perturbations, if observed (e.g., as suggested by Iyemori et al., 2005), would seem to suggest that AWs are a major source of post-seismic magnetic fluctuations (one would not expect piezomagnetic or oceanic sources to generate conjugate perturbations).

These model results presented here represent, to the best of our knowledge, the most detailed, high-resolution, and physics-rich characterization of ionospheric responses to nonlinear AWs generated by EQ. There remain opportunities for improvement; most importantly, to incorporate direct model simulations of the evolving ocean surface and tsunami contributions to AGW sources, leading to more-realistic AGW fields. Nevertheless, the present results demonstrate basis for a complete framework for modeling and interpreting tsunami-related TEC and magnetic perturbations. Equally, for inland EQs, a better characterization of fault rupture dynamics and associated surface waves is necessary. More realistic sources are a subject of our ongoing investigations and will be reported separately. Even with the controlled sources used presently, however, results are both qualitatively and quantitatively consistent with epicentral TEC data analyses presented in Zettergren et al. (2017). Further, they support the hypothesis that reported magnetic fluctuations following very large EQs, including conjugate, are attributable to AW effects in the ionosphere (Iyemori et al., 2005). More-critical comparisons of TEC *and* magnetic field data, together with detailed simulation results, can provide specific new insight and be further-leveraged to understand seismic sources and their effects throughout the earth-atmosphere-ionosphere systems.

References

Amestoy, P. R., Duff, I. S., L'Excellent, J.-Y., & Koster, J. (2001). A fully asynchronous multifrontal solver using distributed dynamic scheduling. *SIAM Journal on Matrix Analysis and Applications*, 23(1), 15–41.

Amestoy, P. R., Guermouche, A., L'Excellent, J.-Y., & Pralet, S. (2006). Hybrid scheduling for the parallel solution of linear systems. *Parallel Computing*, 32(2), 136–156.

Astafyeva, E., Shalimov, S., Olshanskaya, E., & Lognonné, P. (2013). Ionospheric response to earthquakes of different magnitudes: Larger quakes perturb the ionosphere stronger and longer. *Geophysical Research Letters*, 40, 1675–1681. https://doi.org/10.1002/grl.50398

Bale, D. S., LeVeque, R. J., Mitran, S., & Rossmanith, J. A. (2003). A wave propagation method for conservation laws and balance laws with spatially-varying flux functions. *SIAM Journal on Scientific Computing*, 24, 955–978.

Clawpack Development Team (2002). Clawpack software version 4.2. Retrieved from http://www.clawpack.org

Dautermann, T., Calais, E., Lognonné, P., & Mattioli, G. S. (2009). Lithosphere-atmosphere-ionosphere coupling after the 2003 explosive eruption of the Soufriere Hills Volcano, Montserrat. *Geophysical Journal International*, *179*, 1537–1546. https://doi.org/10.1111/j.1365-246X.2009.04390.x

Fritts, D. C., & Alexander, M. J. (2003). Gravity wave dynamics and effects in the middle atmosphere. *Reviews of Geophysics*, *41*(1), 1003. https://doi.org/10.1029/2001RG000106

Fritts, D. C., Vadas, S. L., Wan, K., & Werne, J. A. (2006). Mean and variable forcing of the middle atmosphere by gravity waves. *Journal of Atmospheric and Solar-Terrestrial Physics*, *68*, 247–265. https://doi.org/10.1016/j.jastp.2005.04.010

Galvan, D. A., Komjathy, A., Hickey, M. P., Stephens, P., Snively, J., Tony Song, Y., et al. (2012). Ionospheric signatures of Tohoku-Oki Tsunami of March 11, 2011: Model comparisons near the epicenter. *Radio Science*, *47*, RS4003. https://doi.org/10.1029/2012RS005023

Hao, Y., Xiao, Z., & Zhang, D. (2012). Multi-instrument observation on co-seismic ionospheric effects after great Tohoku Earthquake. *Journal of Geophysical Research*, *117*, A02305. https://doi.org/10.1029/2011JA017036

Hao, Y., Xiao, Z., & Zhang, D. (2013). Teleseismic magnetic effects (TMDS) of 2011 Tohoku Earthquake. *Journal of Geophysical Research: Space Physics*, *118*, 3914–3923. https://doi.org/10.1002/jgra.50326

Hasbi, A. M., Momani, M. A., Mohd Ali, M. A., Misran, N., Shiokawa, K., Otsuka, Y., & Yumoto, K. (2009). Ionospheric and geomagnetic disturbances during the 2005 Sumatran Earthquakes. *Journal of Atmospheric and Solar-Terrestrial Physics*, *71*, 1992–2005. https://doi.org/10.1016/j.jastp.2009.09.004

Huba, J. D., Drob, D. P., Wu, T.-W., & Makela, J. J. (2015). Modeling the ionospheric impact of tsunami-driven gravity waves with SAMI3: Conjugate effects. *Geophysical Research Letters*, *42*, 5719–5726. https://doi.org/10.1002/2015GL064871

Huba, J. D., Joyce, G., & Fedder, J. A. (2000). Sami2 is Another Model of the Ionosphere (SAMI2): A new low-latitude ionosphere model. *Journal of Geophysical Research*, *105*, 23,035–23,054. https://doi.org/10.1029/2000JA000035

Imtiaz, N., & Marchand, R. (2012). Modeling of ionospheric magnetic field perturbations induced by earthquakes. *Journal of Geophysical Research*, *117*, A04320. https://doi.org/10.1029/2011JA017475

Iyemori, T., Nose, M., Han, D., Gao, Y., Hashizume, M., Choosakul, N., et al. (2005). Geomagnetic pulsations caused by the Sumatra earthquake on December 26, 2004. *Geophysical Research Letters*, *32*, L20807. https://doi.org/10.1029/2005GL024083

Johnston, M. (1997). Review of electric and magnetic fields accompanying seismic and volcanic activity. *Surveys in Geophysics*, *18*(5), 441–476.

Kakinami, Y., Kamogawa, M., Tanioka, Y., Watanabe, S., Gusman, A. R., Liu, J., et al. (2012). Tsunamigenic ionospheric hole. *Geophysical Research Letters*, *39*, L00G27. https://doi.org/10.1029/2011GL050159

Kherani, E. A., Lognonné, P., Hébert, H., Rolland, L., Astafyeva, E., Occhipinti, G., et al. (2012). Modelling of the total electronic content and magnetic field anomalies generated by the 2011 Tohoku-Oki Tsunami and associated acoustic-gravity waves. *Geophysical Journal International*, *191*, 1049–1066. https://doi.org/10.1111/j.1365-246X.2012.05617.x

LeVeque, R. J. (2002). *Finite volume methods for hyperbolic problems*. Cambridge, UK: Cambridge University Press.

Li, J. D., Rude, C. M., & Pankratius, V. (2018). Characterizing the complex two N-wave ionospheric signature of the 2016 Kaikoura Earthquake. *Journal of Geophysical Research: Space Physics*, *123*, 10,358–10,367. https://doi.org/10.1029/2018JA025376

Matsumura, M., Saito, A., Iyemori, T., Shinagawa, H., Tsugawa, T., Otsuka, Y., et al. (2011). Numerical simulations of atmospheric waves excited by the 2011 off the Pacific coast of Tohoku earthquake. *Earth, Planets, and Space*, *63*(7), 885–889. https://doi.org/10.5047/eps.2011.07.015

Meng, X., Verkhoglyadova, O. P., Komjathy, A., Savastano, G., & Mannucci, A. J. (2018). Physics-based modeling of earthquake? Induced ionospheric disturbances. *Journal of Geophysical Research: Space Physics*, *123*, 8021–8038. https://doi.org/10.1029/2018JA025253

Peltier, W. R., & Hines, C. O. (1976). On the possible detection of tsunamis by a monitoring of the ionosphere. *Journal of Geophysical Research*, *81*, 1995–2000.

Picone, J. M., Hedin, A. E., Drob, D. P., & Aikin, A. C. (2002). NRLMSISE-00 empirical model of the atmosphere: Statistical comparisons and scientific issues. *Journal of Geophysical Research*, *107*(A12), 1468. https://doi.org/10.1029/2002JA009430

Rolland, L. M., Lognonné, P., & Munekane, H. (2011). Detection and modeling of Rayleigh wave induced patterns in the ionosphere. *Journal of Geophysical Research*, *116*, A05320. https://doi.org/10.1029/2010JA016060

Saito, A., Tsugawa, T., Otsuka, Y., Nishioka, M., Iyemori, T., Matsumura, M., et al. (2011). Acoustic resoinance and plasma depletion detected by GPS total electron content observations after the 2011 off the Pacific coast of Tohoku Earthquake. *Earth, Planets, and Space*, *63*, 863–867. https://doi.org/10.5047/eps.2011.06.034

Shinagawa, H., Tsugawa, T., Matsumura, M., Iyemori, T., Saito, A., Maruyama, T., et al. (2013). Two-dimensional simulation of ionospheric variations in the vicinity of the epicenter of the Tohoku-Oki Earthquake on 11 March 2011. *Geophysical Research Letters*, *40*, 5009–5013. https://doi.org/10.1002/2013GL057627

Snively, J. B. (2013). Mesospheric hydroxyl airglow signatures of acoustic and gravity waves generated by transient tropospheric forcing. *Geophysical Research Letters*, *40*, 4533–4537. https://doi.org/10.1002/grl.50886

Utada, H., Shimizu, H., Ogawa, T., Maeda, T., Furumura, T., Yamamoto, T., et al. (2011). Geomagnetic field changes in response to the 2011 off the pacific coast of Tohoku earthquake and tsunami. *Earth and Planetary Science Letters*, *311*(1), 11–27.

Zettergren, M., Semeter, J., & Dahlgren, H. (2015). Dynamics of density cavities generated by frictional heating: Formation, distortion, and instability. *Geophysical Research Letters*, *42*, 10,120–10,125. https://doi.org/10.1002/2015GL066806

Zettergren, M. D., & Snively, J. B. (2013). Ionospheric signatures of acoustic waves generated by transient tropospheric forcing. *Geophysical Research Letters*, *40*, 5345–5349. https://doi.org/10.1002/2013GL058018

Zettergren, M. D., & Snively, J. B. (2015). Ionospheric response to infrasonic-acoustic waves generated by natural hazard events. *Journal of Geophysical Research: Space Physics*, *120*, 8002–8024. https://doi.org/10.1002/2015JA021116

Zettergren, M., Snively, J., Komjathy, A., & Verkhoglyadova, O. (2017). Nonlinear ionospheric responses to large-amplitude infrasonic-acoustic waves generated by undersea earthquakes. *Journal of Geophysical Research: Space Physics*, *122*, 2272–2291. https://doi.org/10.1002/2016JA023159

Erratum

In the originally published version of this article, Figure 4 was published incorrectly. This error has since been corrected, and this version may be considered the authoritative version of record.